PHYSICAL REVIEW FLUIDS **1**, 032401(R) (2016)

Nonlinear interactions isolated through scale synthesis in experimental wall turbulence

Subrahmanyam Duvvuri* and Beverley McKeon
Graduate Aerospace Laboratories, California Institute of Technology, Pasadena, California 91125, USA
(Received 8 April 2016; published 15 July 2016)

An experimental investigation of nonlinear scale interactions in a forced turbulent boundary layer is presented here. A dynamic wall perturbation mechanism was used to externally force two distinct large-scale synthetic modes with well-defined spatial and temporal wave numbers in a fully turbulent flow. The focus is on characterizing the nonlinear flow response at triadically consistent wave numbers that arises from the direct interactions of the two synthetic modes. These experimental results isolate triadic scale interactions in wall turbulence in a unique fashion, and provide the ability to explore the dynamics of scale coupling in a systematic and detailed manner. The ideas advanced here are intended to contribute towards modeling efforts of high-Reynolds-number wall turbulence.

DOI: 10.1103/PhysRevFluids.1.032401

The dynamics of turbulent flows are characterized by the presence of a wide range of energetic scales with inherent nonlinear coupling. The high-dimensional and nonlinear nature of the problem, as viewed from a systems perspective, makes it innately challenging. Our interest is in wall-bounded turbulent flows, in boundary layers, channels, pipes, etc., where the presence of a bounding surface accentuates the role of fluid viscosity in its vicinity and establishes a mean shear-stress gradient. The resulting nonhomogeneity in the wall-normal direction alters the characteristics of turbulence at a fundamental level and introduces unique considerations that set wall turbulence apart from other classes of turbulent flows. In addition to its scientific importance, the immense practical scope of applications involving wall turbulence continues to drive concerted research efforts involving experimental, theoretical, and computational approaches to the problem [1].

While considerable progress has been made in explaining the linear mechanisms involved in the dynamics of wall turbulence, the nonlinear aspects are often treated indirectly through modeling approaches. The present work is aimed at investigating the dynamics of nonlinear scale coupling at a fundamental level. Consider a fully developed turbulent wall flow with a three-dimensional velocity fluctuation field $\mathbf{u}(x,y,z,t)$, where x,y,z denote the streamwise, wall-normal, and spanwise coordinates, respectively, and t denotes time. We restrict our attention to two distinct scales of motion, denoted by $\tilde{\mathbf{u}}_1$ and $\tilde{\mathbf{u}}_2$, that constitute the velocity field $\mathbf{u}$ together with other scales of turbulence. They are expressed in the form of normal modes, each with positive ($\tilde{\mathbf{u}}^+$) and negative ($\tilde{\mathbf{u}}^-$) complex oblique wave components

$$\begin{aligned}\tilde{\mathbf{u}}_1 &= \hat{\mathbf{u}}_1 e^{i(k_{x1}x+k_{z1}z-\omega_1 t)} + \hat{\mathbf{u}}_1^* e^{-i(k_{x1}x+k_{z1}z-\omega_1 t)} = \tilde{\mathbf{u}}_1^+ + \tilde{\mathbf{u}}_1^-,\\ \tilde{\mathbf{u}}_2 &= \hat{\mathbf{u}}_2 e^{i(k_{x2}x+k_{z2}z-\omega_2 t)} + \hat{\mathbf{u}}_2^* e^{-i(k_{x2}x+k_{z2}z-\omega_2 t)} = \tilde{\mathbf{u}}_2^+ + \tilde{\mathbf{u}}_2^-. \end{aligned} \quad (1)$$

Here $\mathbf{k}_1 = (k_{x1},k_{z1},\omega_1)$ and $\mathbf{k}_2 = (k_{x2},k_{z2},\omega_2)$ denote spatial and temporal wave numbers along the homogeneous directions (x,z,t), respectively.[1] The complex amplitudes $\hat{\mathbf{u}}_j$ (and conjugates $\hat{\mathbf{u}}_j^*$) in the above equation are a function of the nonhomogeneous coordinate y and contain phase information for the modes. It is worth noting that complex exponentials provide the optimal basis functions

*subrahmanyam@caltech.edu

[1]The locally parallel flow approximation is implicitly invoked for a boundary layer flow by treating the statistics of $\mathbf{u}$ to be invariant in the streamwise direction. Results from the present experimental scenario suggest this to be a reasonable approximation for the purposes of this paper.

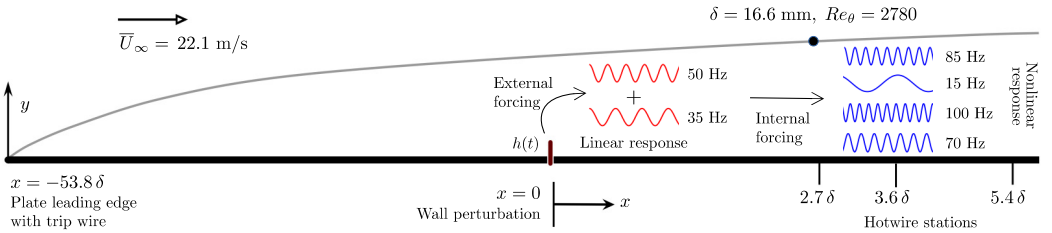

FIG. 1. Schematic of the flat plate setup (not to scale). A thin spanwise-aligned straight rib is positioned at the wall ($x = 0$) and actuated in the wall-normal direction to force the flow simultaneously at two frequencies. Phase-locked hot-wire anemometer measurements were made at three downstream ($x > 0$) stations as marked. The BL thickness δ and Reynolds number Re_θ for the flow at station 1 ($x = 2.7\delta$) are indicated; only a minor increase in these quantities was noted over the range $0 < x < 5.4\delta$.

(energy norm) for decomposition of the velocity field in the homogeneous directions and thus are routinely employed in descriptions of turbulent flow fields that possess some degree of translational invariance. For instance, the resolvent operator model [2] exploits the low-rank nature of linear dynamics that results from such a decomposition to successfully capture some key features of wall turbulence. In addition to its attractive mathematical properties, the Fourier basis provides a clear and simple quantitative definition of scale in terms of a wave number $\mathbf{k}_j$.

We now consider the nature of interaction between the two modes $\tilde{\mathbf{u}}_1$ and $\tilde{\mathbf{u}}_2$ and begin by noting that the nonlinear convective acceleration term $(\mathbf{u}\cdot\nabla)\mathbf{u}$ in the governing Navier-Stokes equation is quadratic in $\mathbf{u}$. The implications of this are readily seen from Eq. (1): Quadratic interactions between wave components $\tilde{\mathbf{u}}_1^+, \tilde{\mathbf{u}}_1^-, \tilde{\mathbf{u}}_2^+, \tilde{\mathbf{u}}_2^-$ establish a direct coupling between the modes under consideration and their sum and difference wave-number modes, denoted by $\tilde{\mathbf{u}}_3$ and $\tilde{\mathbf{u}}_4$, with wave numbers $\mathbf{k}_3 = \mathbf{k}_1 + \mathbf{k}_2$ and $\mathbf{k}_4 = \mathbf{k}_1 - \mathbf{k}_2$, respectively. Also, self-interactions of $\tilde{\mathbf{u}}_1$ and $\tilde{\mathbf{u}}_2$ establish a direct coupling with their respective harmonic modes, denoted by $\tilde{\mathbf{u}}_5$ and $\tilde{\mathbf{u}}_6$, with wave numbers $\mathbf{k}_5 = 2\mathbf{k}_1$ and $\mathbf{k}_6 = 2\mathbf{k}_2$. Such sets of three wave numbers $\{\mathbf{k}_1, \mathbf{k}_2, \mathbf{k}_3\}$ and $\{\mathbf{k}_1, \mathbf{k}_2, \mathbf{k}_4\}$ are said to possess triadic consistency, with harmonic wave-number sets like $\{\mathbf{k}_1, \mathbf{k}_1, \mathbf{k}_5\}$ and $\{\mathbf{k}_2, \mathbf{k}_2, \mathbf{k}_6\}$ being the self-interaction cases. The coupling between triadically consistent wave numbers, referred to as triadic interactions, is a key aspect of the flow dynamics from which the observed statistics and structure of wall turbulence emanate. A forcing-response-type approach is used here to experimentally study triadic interactions in a turbulent boundary layer. Two distinct spatiotemporal modes are externally forced, or excited, and the linear and nonlinear responses of the flow are measured and analyzed.

A flat plate zero-pressure-gradient boundary layer (BL) flow was forced by a spatially impulsive dynamic wall perturbation; the flow has a constant free-stream velocity of $\overline{U}_\infty = 22.1$ m/s and is fully turbulent at the perturbation location with a layer thickness $\delta \approx 16.6$ mm and momentum thickness Reynolds number $\mathrm{Re}_\theta \approx 2780$ (see Fig. 1). The wall perturbation geometry was adapted from earlier experiments [3,4] and consists of a thin straight rib of thickness 1.5 mm aligned along the spanwise direction. The rib is connected to a linear motor mechanism placed underneath the plate; a plate insert allows for smooth rib reciprocation in the wall-normal direction. The rib is actuated by the motor with a waveform consisting of two frequency components, given by

$$h(t)/\delta = a[2 + \cos(\omega_1 t) + \cos(\omega_2 t)], \tag{2}$$

where $h(t)/\delta$ is the instantaneous nondimensional height (y location of the rib) with $h = 0$ corresponding to the wall. The following amplitude and frequency values were chosen for the experiment: $a = 0.024$, $\omega_1/2\pi = 50$ Hz, and $\omega_2/2\pi = 35$ Hz. Note that the maximum instantaneous height of the rib is around 10% of the local BL thickness; $h_{\max} = 0.096\delta$ and $h_{\mathrm{rms}} \approx 0.054\delta$ from Eq. (2). The entire actuation mechanism was carefully tuned to ensure that the rib displacement closely matched Eq. (2); the same was confirmed by measurements of the actual rib displacement obtained from a linear encoder. The overall quality of the flow setup was found to be satisfactory

with no vibration or noise contamination in the tunnel test section. Phase-locked measurements of time-resolved streamwise velocity U were made using a hot-wire anemometer at three different measurement stations downstream of the perturbation (marked in Fig. 1). At each measurement station the wall-normal flow profile was sampled at 50 logarithmically spaced locations between $y = 0.008\delta$ and 3δ, with sufficient temporal resolution to fully resolve the turbulence spectrum at all locations. Measurements were also made of the canonical flow (smooth flat plate without the perturbation) for reference and were found to be in satisfactory agreement with previous literature. The BL thickness and Reynolds number grow at a very slow pace in the region of interest ($0 < x < 5.4\delta$) and hence are treated to be constants for the purposes of the present analysis. Also, in comparison with the canonical flow, no significant changes in δ or Re_θ were noticed in the presence of the dynamic forcing in the region of measurements. An estimate of friction Reynolds number Re_τ for the flow is made from Re_θ using the Coles-Fernholz empirical relationship to be $\mathrm{Re}_\tau \approx 940$; the friction length scale, or inner scale, ν/u_τ (ν is the kinematic viscosity of air and u_τ is the friction velocity) thus obtained is used along with the outer scale δ for reference in later figures. However, it is important to note that the estimate of Re_τ is strictly valid only for the canonical flow. Interested readers are referred to [5] for a more detailed description of the experiment.

Before proceeding to the results, we make the following remarks with regard to the experimental design. A spanwise-constant perturbation results in nominally two-dimensional (2D) disturbances (x-y plane) and was chosen for ease in experimentation. The choice of perturbation frequencies and amplitudes was guided by the objective of targeting the large-scale region of the turbulence spectrum. The significance of large-scale fluctuations, particularly the very-large-scale motions (VLSMs), on the overall flow dynamics is increasingly clear [6] and hence they are a natural starting point for attempts at understanding the complex network of coupled spatiotemporal scales of wall turbulence. The large scales also present a practical avenue to experimentally effect external perturbations (or forcing) on the flow, particularly at high Reynolds numbers. Previous work by Jacobi and McKeon [3] and by the present authors [4] demonstrates the effectiveness of a spatially impulsive wall perturbation in forcing a single synthetic large-scale mode. The 50-Hz component in the present case was chosen to match [4] and a 35-Hz component was added to simultaneously force another distinct large-scale mode. The combination of these frequencies results in triadic responses with no duplication and sufficient separation in the turbulence spectrum (see results). Finally, the amplitude a was chosen to induce disturbances of sufficient strength in the downstream region while keeping the blockage effects associated with the rib to a minimum. We now proceed to the experimental results and model the wall-perturbation-induced disturbances as spanwise-constant ($k_z = 0$) normal modes.

Time-resolved streamwise velocity from the anemometer is decomposed into local mean and fluctuating components $U(y,t) = \overline{U}(y) + u(y,t)$. A slight deficit in the mean momentum relative to the canonical flow, brought about by blockage effects of the rib and also possibly due to the dynamic forcing effects, was observed in the logarithmic region (see [5]). Since our interest is in the triadic interactions associated with the synthetic modes, we restrict our attention to the fluctuations. The power spectral density (PSD) Φ of u provides the distribution of energy across temporal scales; Φ is calculated using the standard Welch method and is shown in Fig. 2(a) as a function of frequency f at station 1 ($x = 2.7\delta$). Linear flow response to external forcing in the large-scale region can immediately be seen at $f_1 = 50$ Hz and $f_2 = 35$ Hz in the form of energetic narrow-band vertical streaks. The two-frequency dynamic forcing excites two distinct large-scale motions, referred to as the forcing modes,[2] with frequencies f_1 and f_2. From the earlier discussion of triadic coupling, the interactions between the two forcing modes is expected to result in direct nonlinear response with some degree of coherence. A closer inspection of Fig. 2(a) reveals what is perhaps the most striking feature of this experiment: A clear energetic response is seen at the sum

[2]Note that the use of terminology "forcing modes" in the present context differs from that of the resolvent operator framework [2].

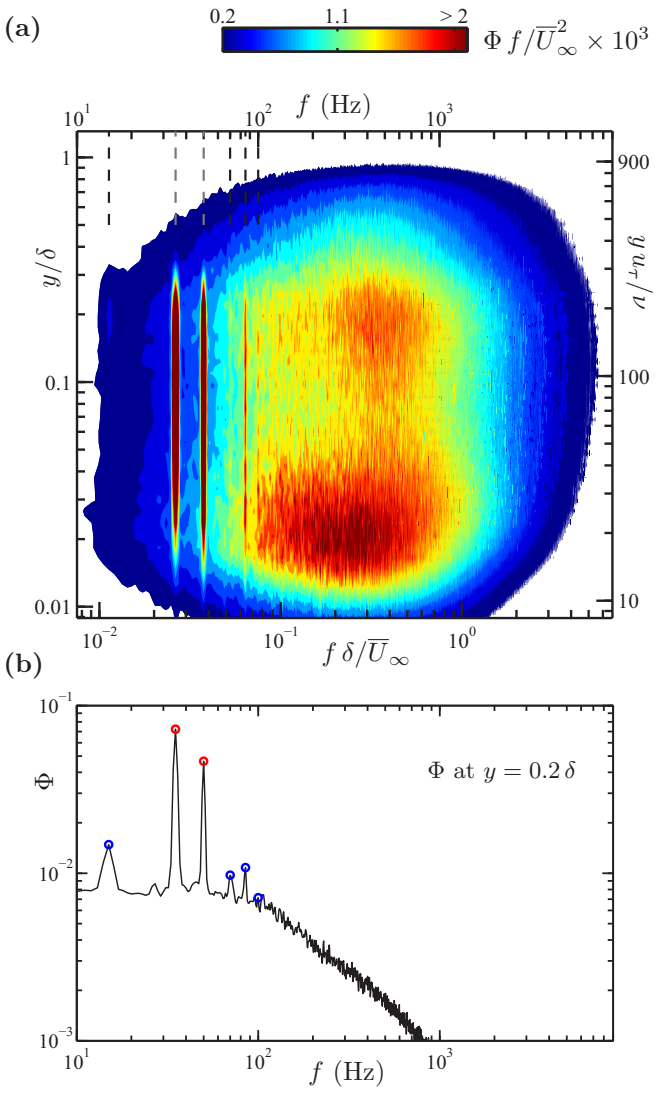

FIG. 2. (a) Premultiplied and scaled power spectral density of streamwise velocity fluctuations at station 1. Dashed vertical lines indicating the forcing (gray) and response (black) frequencies are shown for reference. (b) Raw power spectral density at $y = 0.2\delta$ from the above composite spectrum is shown to highlight the amplitude peaks at the frequencies of interest. Round markers in red and blue indicate the forcing and response frequencies, respectively. There seems to be no increase in the power level of $f_5 = 100$ Hz at this wall-normal location.

frequency $f_3 = f_1 + f_2 = 85$ Hz spanning a significant region in the BL. The nonlinear interaction between the externally forced frequencies gives rise to internal forcing at f_3 that results in a noticeable increase in power level (or intensity). A similar response is also noted at the difference frequency $f_4 = f_1 - f_2 = 15$ Hz and harmonics $f_5 = 2f_1 = 100$ Hz and $f_6 = 2f_2 = 70$ Hz, though not visually prominent in the premultiplied spectra. The raw PSD curve at $y = 0.2\delta$ is shown separately in Fig. 2(b) as an example to highlight these frequency peaks. The triadic response modes, with frequencies f_3, f_4, f_5, and f_6, are referred to simply as response modes. It is important to note at this point that the amplitude and phase behavior of the response modes is dictated by the dynamics

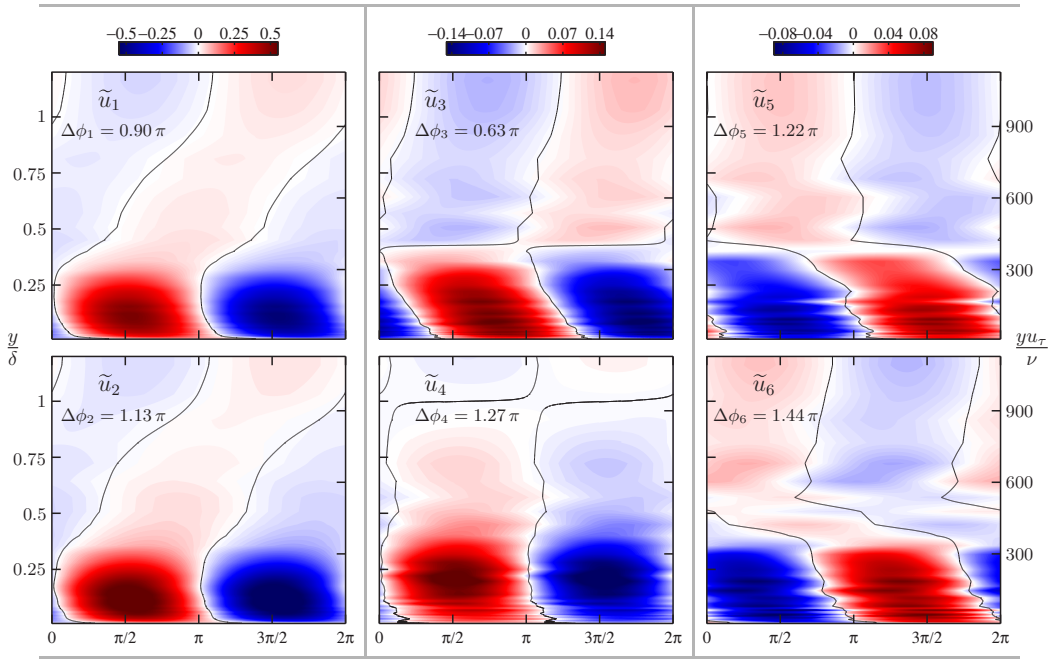

FIG. 3. Amplitude and phase maps $\tilde{u}(y,t)$ for modes of interest over one corresponding temporal period of oscillation at station 1. Color levels are in raw velocity units (m/s). The left column shows the forcing modes $\tilde{u}_1$ and $\tilde{u}_2$, the middle column the sum and difference response modes $\tilde{u}_3$ and $\tilde{u}_4$, and the right column the harmonic response modes $\tilde{u}_5$ and $\tilde{u}_6$. Contour lines, approximately indicating $\tilde{u} = 0$, highlight phase variation with wall-normal distance. Note that constant phase shifts $\Delta\phi_j$ were applied across y in each panel for better presentation. The data shown correspond to the streamwise component of the mode velocity $(\tilde{\mathbf{u}}_j^+)e^{i(\Delta\phi_j)} + (\tilde{\mathbf{u}}_j^-)e^{i(-\Delta\phi_j)}$; values chosen for constants $\Delta\phi_j$ are indicated in the respective panels.

of the particular set of triadic scales under consideration and there is no simple way to predict them *a priori*. Direct coupling between scales in itself does not necessitate net energy transfer in the presence of external forcing.

Having seen clear evidence of forced triadic interactions from the frequency spectra, we now seek to obtain spatial length scales and characterize the phase behavior of the two forcing modes and the corresponding triadic response modes. Velocity measurements phase locked to the input signal [rib displacement $h(t)$ obtained from the linear encoder] allow us to carefully isolate frequency components of interest from a turbulent signal. A phase-averaging scheme was developed and implemented to construct coherent amplitude and phase maps of the synthetic modes from measurements at various wall-normal locations; only the final results are shown here; see [5] for the detailed procedure. Figure 3 shows streamwise components $\tilde{u}_j$ over one period for the forcing and response modes constructed using data from station 1. Similar constructions were made using data from the other two downstream stations (not shown here) and by tracking the change in the phase of each mode with streamwise distance their spatial length scales were estimated. Table I shows the streamwise wave numbers k_x (and corresponding wavelengths $\lambda_x = 2\pi/k_x$); note that this is actual spatial information obtained from measurements at multiple x locations without any assumptions about the mode convection velocity (such as Taylor's hypothesis). Triadic relationships between the spatial wave numbers can be verified with these data; we have $k_{x3}(=0.74\delta^{-1}) \approx k_{x1} + k_{x2}(=0.75\delta^{-1})$, $k_{x4}(=0.12\delta^{-1}) \approx k_{x1} - k_{x2}(=0.11\delta^{-1})$, $k_{x5}(=0.84\delta^{-1}) \approx 2k_{x1}(=0.86\delta^{-1})$, and $k_{x6}(=0.66\delta^{-1}) \approx 2k_{x2}(=0.64\delta^{-1})$. The slight differences are within the experimental uncertainty involved in estimation of the spatial wavelengths. With that we have triadic consistency among the wave-number triplets $\mathbf{k}$, i.e., $\mathbf{k}_3 = \mathbf{k}_1 + \mathbf{k}_2$, $\mathbf{k}_4 = \mathbf{k}_1 - \mathbf{k}_2$, $\mathbf{k}_5 = 2\mathbf{k}_1$,

TABLE I. Spatiotemporal wave numbers and wave speeds for the forcing and triadic response modes.

Mode	$\omega\delta/\overline{U}_\infty$	$k_x\delta$ (λ_x/δ)[a]	$c/\overline{U}_\infty$
$\tilde{\mathbf{u}}_1$	0.24	0.43 (14.6)	0.56
$\tilde{\mathbf{u}}_2$	0.17	0.32 (19.8)	0.53
$\tilde{\mathbf{u}}_3$	0.41	0.74 (8.5)	0.55
$\tilde{\mathbf{u}}_4$	0.07	0.12 (54.2)	0.58
$\tilde{\mathbf{u}}_5$	0.48	0.84 (7.5)	0.57
$\tilde{\mathbf{u}}_6$	0.34	0.66 (9.5)	0.52

[a]The experimental uncertainty in the estimates of λ_x is $\sim\pm 1\delta$.

and $\mathbf{k}_6 = 2\mathbf{k}_2$. These observations suggest that the disturbances excited by the wall perturbation are described reasonably well by a normal mode model. It is noted that the wave numbers k_x are not purely real and have a complex component associated with amplitude decay in the streamwise direction. Since the forcing is applied in a spatially impulsive manner a finite decay rate is observed and can be easily quantified (see [5]). Mode convection velocities, or wave speeds c ($=\omega/k_x$), are also shown in Table I. It is observed that the two forcing modes excited by the wall perturbation propagate downstream at nearly the same speed, i.e., $c_1 \approx c_2$. The two spatiotemporal modes can thereby be interpreted as being part of a single physical coherent structure generated by the perturbation, propagating downstream at roughly 55% of the free-stream velocity. The triadic response modes, by implication, also propagate downstream at nearly the same speeds. The flow consists of two dominant forcing modes and four triadic response modes and this six-mode structure possesses a good degree of coherence in space and time downstream of the perturbation.

We now make brief qualitative observations with reference to Fig. 3 on the amplitude and phase characteristics of the forcing and response modes. The two forcing modes $\tilde{u}_1$ and $\tilde{u}_2$ exhibit almost identical behavior, characterized by a gradual phase change of π rad going from the near-wall region to the BL edge, and closely match the single synthetic mode reported in Ref. [4]. The similarity in the linear flow response is not entirely surprising given the identical nature of external forcing applied at two frequencies that are nearby in spectral space. Moving to the response modes, an interesting contrast between the sum and difference wave-number modes $\tilde{u}_3$ and $\tilde{u}_4$ is noted. Starting at the wall, $\tilde{u}_3$ has a backward phase tilt in time t (forward leaning in streamwise direction x) followed by an abrupt phase jump of π rad at $y \approx 0.4\delta$, reminiscent of critical layer mechanisms in 2D normal mode instability of a laminar inviscid boundary layer [7]. The direction of tilt is then found to be reversed above the phase jump location. In comparison, $\tilde{u}_4$ is vertically aligned for the entire height and exhibits a π-rad phase jump at the BL edge. The contrasting behavior between the two triadic response modes can be attributed to a combination of two factors. First, the two modes have disparate streamwise length scales. The difference response mode $\tilde{u}_4$ is found to be extremely long with a streamwise wavelength of approximately 50δ; longitudinal confinement effects[3] of the wind tunnel test section could potentially be significant at these length scales and deviations from normal mode behavior are to expected. In addition to this experimental limitation, the structure of internal nonlinear forcing from the synthetic modes is different at the sum and difference wave numbers, hence contrasting behaviors are to be expected. Finally, it is noted that the harmonic modes $\tilde{u}_5$ and $\tilde{u}_6$ look similar, and from the above discussion this can be attributed to the nearly identical nature of the forcing modes $\tilde{u}_1$ and $\tilde{u}_2$. The results seem to suggest that the harmonic modes exhibit a π-rad phase jump at $y \approx 0.4\delta$ similar to the sum or difference wave-number modes, but with the opposite sense. While this is an interesting observation, it is important to take note of the relative mode intensities at this point. The harmonic modes are weaker than the sum and difference wave-number modes, which in turn are weaker than the forcing modes (compare colorbar levels in Fig. 3). The drop in

[3]The trailing edge airfoil on the flat plate is roughly 92δ downstream of the wall perturbation ($x = 0$).

intensity has a bearing on the results of the phase-averaging procedure where the accuracy decreases with mode intensity; this is reflected in the increased phase jitter going from panel columns 1 to 3 in Fig. 3. Therefore, further scrutiny is required for proper interpretation of the π-rad phase jump exhibited by the harmonic modes. The data presented here allow for a more detailed analysis of the phase relationships between triadically coupled scales and this is a subject of ongoing work.

These results demonstrate the effectiveness of a forcing-response type approach towards understanding the dynamical structure of wall turbulence. Deterministic external inputs to the flow provide the ability to highlight specific scales and then carefully study the nature of their nonlinear coupling with other scales of turbulence. Parallels can be drawn with regard to the dynamics of mode interactions between the present work and ideas previously developed in the context of laminar BL transition (for instance [8]) and receptivity to freestream disturbances [9]. However, a fully developed turbulent flow presents a much more complicated scenario with a rich set of dynamics over a wide range of scales. While the focus of this paper has been on the direct interactions between the two externally forced large-scale modes, we note that their influence propagates further through secondary interactions, tertiary interactions, and so on. Also, the presence of energetic coherent large scales in the flow has an influence on the small-scale activity. For instance, it manifests as a phase-locking effect on the small scales in the presence of a single energetic scale [4]. The long-term goal of this line of investigation is to aid modeling efforts towards building a *closed picture* of the network of interacting scales in wall turbulence. A robust model of wall turbulence thus derived could potentially enable practical manipulation of energetic turbulence through targeted large-scale inputs by capitalizing on the dynamics of nonlinear scale coupling.

We gratefully acknowledge AFOSR (Grant No. FA 9550-12-1-0469, program manager D. Smith) for financial support of this work and a graduate fellowship (S.D.) from the Resnick Institute at Caltech. We also thank K. Rosenberg and D. Huynh for their help with the wind tunnel experimental setup.

[1] A. J. Smits and I. Marusic, Wall-bounded turbulence, Phys. Today **66**(9), 25 (2013).

[2] B. J. McKeon and A. S. Sharma, A critical-layer framework for turbulent pipe flow, J. Fluid Mech. **658**, 336 (2010).

[3] I. Jacobi and B. J. McKeon, Dynamic roughness perturbation of a turbulent boundary layer, J. Fluid Mech. **688**, 258 (2011).

[4] S. Duvvuri and B. J. McKeon, Triadic scale interactions in a turbulent boundary layer, J. Fluid Mech. **767**, R4 (2015).

[5] S. Duvvuri, Non-linear scale interactions in a forced turbulent boundary layer, Ph.D. thesis, California Institute of Technology, 2016.

[6] A. J. Smits, B. J. McKeon, and I. Marusic, High-Reynolds number wall turbulence, Annu. Rev. Fluid Mech. **43**, 353 (2011).

[7] C. C. Lin, *The Theory of Hydrodynamic Stability* (Cambridge University Press, Cambridge, 1955).

[8] J. D. Crouch and T. Herbert, Nonlinear evolution of secondary instabilities in boundary-layer transition, Theor. Comput. Fluid Dyn. **4**, 151 (1993).

[9] W. S. Saric, H. L. Reed, and E. J. Kerschen, Boundary-layer receptivity to freestream disturbances, Annu. Rev. Fluid Mech. **34**, 291 (2002).